Supporting information

Microcosmic Modulation of Co-N Bonding Structure Improves Multi-Function Electrocatalysis Performance

Wenhui Deng[a], Tianjing Wu[a*], Yufeng Wu[a], Fang Chen[a], Yansong Bai[a], Xiaoqing Zou[a], Mingjun Jing[a*], Wentao Deng[b], Hongshuai Hou[b], Xianyou Wang[a]

[a]National Base for International Science & Technology Cooperation, National Local Joint Engineering Laboratory for Key Materials of New Energy Storage Battery, Key Laboratory of Environmentally Friendly Chemistry and Application of Ministry of Education School of Chemistry, Hunan Province Key Laboratory of Electrochemical Energy Storage & Conversion School, of Chemistry Xiangtan University, Xiangtan 411105 (China)

[b]State Key Laboratory of Powder Metallurgy, College of Chemistry and Chemical Engineering, Central South University, Changsha 410083 (China)

[*]Corresponding author. E-mail: twu@xtu.edu.cn; jingmingjun@xtu.edu.cn

Table of Contents

Section S1: Synthetic Section 3
1.1 Raw Materials 3
1.2 Sample Preparation 3
1.3 Characterizations 5
1.4 Electrochemical Measurements 6
1.5 Liquid and Quasi-Solid-State Zn-Air Batteries 7
1.6 Theoretical Calculations 8
Section S2 Theoretical design 9
2.1 The mechanism of the OER and ORR process 9
Section S3: Material Characterizations 10
3.1 The various colors of the molecular catalyst 10
3.2 FT-IR and UV/Vis spectra characterizations 11
Section S4 Electrochemical Characterizations 12
4.1 ORR and OER curves of M-PTAPP 12
4.2 CV tests in in N_2- or O_2-saturated alkaline electrolytes 13
4.3 The number of electron transfers 14
4.4 ORR performance of Co-PTAPP and FeCo-PTAPP 15
4.5 Methanol tolerance 16
4.6 The effective surface of Fe-PTAPP and Co-PTAPP 17
4.7 The bifunctional activities 18
4.8 Tafel slopes 19
4.9 The stability test of Co-PTAPP molecular catalyst 20
4.10 The SEM images of Co-PTAPP material before and after testing 21
4.11 The mapping images of Co-PTAPP catalyst after the OER test 22
4.12 The cell performance of the PTAPP, Ni-PTAPP, and Co-PTAPP 23
4.13 Water absorption process of HOEtMImCl 24
4.14 Water uptake value of HOEtMImCl 25
Table S1. Comparison of electrocatalytic performances between Zn-NC/GD sample and recently reported electrocatalysts applied in Zn-air batteries 26
References 27

Section S1: Synthetic Section

1.1 Raw Materials

Pyrrole, P-nitrobenzoic acid, Acetic anhydride, Propanoic acid, $SnCl_2.2H_2O$, Trifluoroacetic acid (TFA), benzene-1,4-dialdehyde (BDA) and Nitrobenzene (NBZ) are obtained by Energy Chemical Co., Ltd. Ammonium hydroxide, Pyridine, Ammonium persulphate (APS), N, N-Dimethylformamide (DMF), $Fe(NO_3)_2.9H_2O$, $Co(NO_3)_2.6H_2O$, $Ni(NO_3)_2.6H_2O$, and $Cu(NO_3)_2$ are provided from Sinopharm Chemical Reagent Co., Ltd. Hydrochloric Acid, KOH are purchased from Hunan Huihong Reagent Co., Ltd. Pt/C (20 wt%) is obtained from Sigma-Aldrich Chemical Regent Co., Ltd. Nafion (5 %) are bought from DuPont. All the reagents are not purified.

1.2 Sample Preparation

The 5,10,15,20-tetrakis(4-nitrophenyl)porphyrin (TNPP): A mixture of p-nitrobenzaldehyde (4.6 g, 30.4 mmol), acetic anhydride (5 mL) and propionic acid (125 mL) is placed into a three round-bottom flask. The flask performs the sealing treatment, followed by three flushed with nitrogen gas. Then the reaction mixture is gradually heated to the reflux. The new steamed pyrrole (2.0 mL, 28.8 mmol) slowly drops into the reaction liquid and stirred for 40 min. After stirring at boiling point for 40 min, the product is collected by filtration and washed with deionized (DI) water. Next, the dry crude products and pyridines are put into the flask and then refluxed for 40 min. When the liquid reached room temperature, the synthetic material is separated by filtration

and washed thoroughly with acetone until the filtrate is colorless. The purple product is obtained by drying at 60 ℃ under a vacuum oven for 12 h.

The 5,10,15,20-tetrakis(4-nitrophenyl)porphyrin (TAPP): The obtained residue is dissolved in 10 M HCl solution and stirred for 10 min at protective gas. 3.10 g of $SnCl_2.2H_2O$ is dispersed in 10 M HCl (10 mL). The dispersed solution is injected into the reaction liquid and then refluxed for 45 min. When the reaction system reached room temperature, the PH of the reaction liquid is adjusted to alkalescence using ammonium hydroxide in an ice bath. The as-prepared purple-like crystalline material is separated by 8000 rpm centrifuge and washed with DI water three times. Then the product is dried overnight at 60 ℃ under a vacuum oven. The solid sample is dissolved in acetone solvent and extracted the purple liquid. The TAPP is collected after removing the solvent.

The poly(5,10,15,20-tetrakis(4aminophenyl)porphyrin) (PTAPP): In the preparative process, 0.10 g of TAPP (0.148 mmol) is dispersed in 100 mL dilute HCl solution (1 M) at 40 ℃ using a stirrer and ultrasound for 20 min to form a green homogenous dispersion. After the water bath temperature at 40 ℃, 0.34 g of APS (1.48 mol) is added into the above green solution under vigorous stirring for 10 min. Then, the reaction is maintained for 1 day without stirring at 40 ℃. The black PTAPP is filtered and washed with dilute HCl solution (1 M) for five times with 100 mL. The purple product is obtained by drying at 60 ℃ under a vacuum oven for 12 h.

The metal-TAPP (M-TAPP): TAPP, $Co(NO_3)_2.6H_2O$ (1.48 mmol), and DMF (20 mL) are mixed in a flask. The mixing product refluxed for 4 h and then removed the solvent.

The reaction product is filtered and washed with 800 mL DI water.

The metal-PTAPP (M-PTAPP): A mixture of PTAPP, $Co(NO_3)_2.6H_2O$ (1.48 mmol), and DMF (20 mL) is placed in a flask. The mixing product refluxed for 4 h and then removed the solvent. The reaction product is filtered and washed with 800 mL DI water. The product was finally dried in a vacuum oven at 60 ℃ for 12 h. At the same condition, the nitrate is changed to $Fe(NO_3)_2.9H_2O$, $Ni(NO_3)_2.6H_2O$, and $Cu(NO_3)_2$, and the products are named Fe-PTAPP, Ni-PTAPP, and Cu-PTAPP.

The Co-porphyrin organic covalent (Co-POC): 1.34 g BDA (10 mmol) is dissolved in propionic acid solution and stirred for 10 min. 5 mL NBZ and 1mL TFA are added to the above solution and then refluxed at 130℃. Subsequently, pyrrole (1.39 mL, 20 mmol) is slowly dripped into the reaction solution. The mixture is continued with stirring and kept at 130°C for 12 h. The product is filtered and washed with ethanol, chloroform, and ethanol to remove unreacted reagents. POC was finally obtained after being dried at 60 °C for 12 h. A mixture of POC, $Co(NO_3)_2.6H_2O$ (1.48 mmol), and DMF (20 mL) is placed in a flask. The mixing product refluxed for 4 h and then removed the solvent. The reaction product is filtered and washed with 800 mL DI water.

1.3 Characterizations

The external morphology of the as-prepared molecular material is displayed via a scanning electron microscope (SEM, JEOL-6700F), which is executed at 10 KV. Transmission electron microscopy (TEM) is applied using a JEM-2100F at 200 KV. The crystallization degree of the materials is elucidated by an X-ray diffractometer

(XRD, D8 DISCOVER diffractometer). The porosity of the prepared samples is assessed through the nitrogen adsorption-desorption tests (TriStar II 3020 2.00). The Fourier transforms infrared (FT-IR) are recorded on a Thermo Scientific Nicolet 6700. The Raman spectrum is carried out using the Renishaw InVia system with the excitation laser (λ) of 532 nm.

1.4 Electrochemical Measurements

The electrocatalytic activity is assessed through the CHI660e electrochemical working station (Chen Hua, Shanghai, China) and the rotating disk electrode (ATA-1B). The testing method is performed using a three electrodes system. In the system, Ag/AgCl (saturated KCl electrolyte) and platinum sheet are employed as reference and counter electrodes, respectively. All potential is transformed into the RHE ($E_{RHE} = E_{Ag/AgCl} + 0.197\ V + 0.059\ pH$). 2.5 mg catalyst and 2.5 mg acetylene black are dispersed in 0.96 mL (isopropanol/H_2O = 5:1, v/v) solution and 0.5 wt% Nafion solution (40 μL), followed by ultrasonic 30 min to form an ink catalyst. A certain volume of catalyst ink is dropped onto a glass carbon (0.708 mg cm^{-2}) or carbon paper (1.0 mg cm^{-2}). The chronoamperometry test is investigated at a constant potential (0.3653 V) with a continuous rotation.

For the ORR activity measurements, the CV measurements are measured in N_2- and O_2-saturated 0.1 M KOH solution at 50 mV s^{-1} from 0.2 V to 2.0 V. LSVs are tested with different rotating speeds from 400 rpm to 2000 rpm).

The OER activities are investigated by LSV in O_2-saturated 1.0 M KOH medium and corrected by 90% iR compensation.

The HER activities are assessed via LSV in N_2-saturated 1.0 M KOH solution.

The electron transfer number (n) can be calculated by Koutecky-Levich (K-L) equation:

$$\frac{1}{j}=\frac{1}{j_L}+\frac{1}{j_k}=\frac{1}{B\sqrt{\omega}}+\frac{1}{j_k} \quad (1)$$

$$B=0.62nFC_0(D_0)^{2/3}\gamma^{-1/6} \quad (2)$$

Where j is assigned the measured current density, j_k and j_l are the kinetic current density and diffusion-limited current density. ω represents the rotation rate (rpm min^{-1}). F shows the Faraday constant (F = 96485 C mol^{-1}). C_0 is the oxygen concentration (solubility) in 0.1 M KOH solution (C_0 = 1.2 × 10^{-3} mol l^{-1}), D_0 is the diffusion coefficient of O_2 (D_0 = 1.9 × 10^{-5} cm^2 s^{-1}), and ν is the kinetic viscosity of the electrolyte (1 × 10^{-2} cm^2 s^{-1}).

1.5 Liquid and Quasi-Solid-State Zn-Air Batteries

To evaluate the catalytic activity of the molecular catalyst, Liquid Zn-air batteries (ZABs) are built, which are assembled with polished Zn plate as anode and catalyst material coated onto carbon cloth as air cathode (2 mg cm^{-2}). The electrolyte is 6.0 M KOH containing 0.2 M Zn $(Ac)_2$. The voltage-current discharge polarization is determined through the LSV curves from 1.6 V – 0 V, which is performed at 5 mV s^{-1} with CHI 660E electrochemical workstation. And, the open-circuit voltage also is measured in CHI 660E electrochemical workstation. Beyond that, other tests are collected by a Neware CT-4008-5V1A-S1 multichannel battery testing system.

To construct flexible ZABs, the pre-cleaned carbon cloth of the loaded catalyst is

employed as the air cathode. The Zn foil is utilized as the anode. The PVA-IL gel is used as a hydrogel electrolyte. To prepare the PVA-IL gel, 1 g 1-hydroxylethy-3-methylimidazolium chloride (HOEtMImCl) powder is uniformly dispersed in 10 mL DI water, then 1 g PVA is added into the above solution and refluxed at 95℃. Next, 1 mL 9 M KOH with 0.2 M Zinc acetate is slowly dipped into the PVA solution with continuous stirring for 40 min. The mixture is poured into the mold at -20 °C for 12 h. For comparison, The PVA hydrogel electrolyte was obtained by the same procedures of the PVA-IL preparation method without the HOEtMImCl additives.

1.6 Theoretical Calculations

The density functional theory (DFT) calculations of catalytic energies are implemented using the Vienna *ab initio* simulation package (VASP5.4.4) code.[1] The exchange-correlation function is fitted with Perdew-Burke-Emzerhof (PBE) functional and the projector augmented wave (PAW) method is used for the ionic core.[2, 3] The long-range van der Waals (vdWs) interaction is analyzed by the DFT-D3 approach.[4] The Monkhorst-Pack k-points grids are employed as 1×1×1 for all non-periodic structures. In addition, the plane wave cutoff energy is set as 400 eV for all calculations. The convergence criteria of 10^{-4} and the force convergency of 0.01 eV A^{-1} are adopted.

The Gibbs free energy (ΔG) is derived from the following equation.

$$\Delta G = \Delta E + \Delta E_{\mathrm{ZPE}} + \Delta H_{0\to T} - T\Delta S + G_{\mathrm{U}} \quad (1)$$

Herein ΔE is the changes of the total energy. The ΔE_{ZPE} expresses zero-point energy. ΔS represent the entropic changes. The $\Delta H_{0\to T}$ is considered to the change of enthalpy from 0 K to T K. Moreover, The G_{U} is the correction from inner energy.

Section S2 Theoretical design

2.1 The mechanism of the OER and ORR process

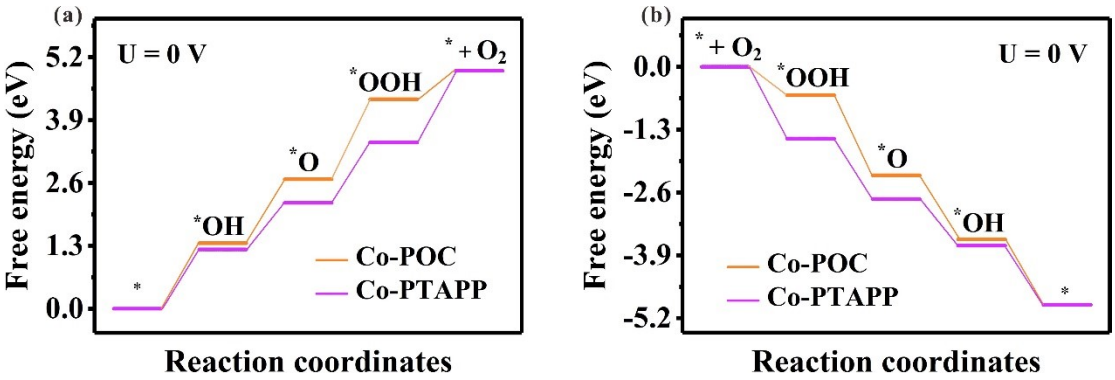

Figure S1. The free energy pathway of Co-POC and Co-PTAPP for (a) OER and (b) ORR at U = 0 V.

For OER (Figure S1a), the four pathways on Co-N_2 and Co-N_4 configurations tends to gradually rise at U = 0 V. For the reverse reaction, the free-energy pathways of as-prepared material is exothermic and spontaneous processes (Figure S1b).

Section S3: Material Characterizations

3.1 The various colors of the molecular catalyst

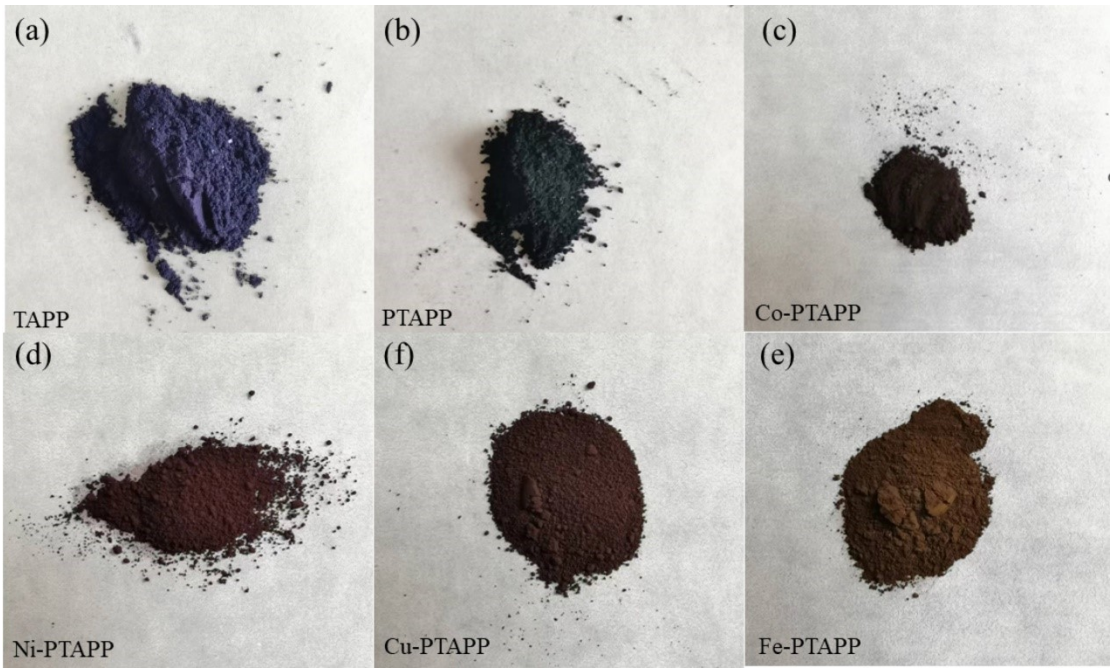

Figure S2. (a-e) External characteristic image of TAPP, PTAPP, and M-PTAPP.

After oxidative polymerization of the TAPP monomer, the color also changed from purple to black, indicating the formation of polymer material. (Figure S2a, b) As revealed in Figure S2c-e, the introduce of the different metal can cause the abundant color (Co-PTAPP : dark brown, Ni-PTAPP : puce, Cu-PTAPP and Fe-PTAPP : brown).

3.2 FT-IR and UV/Vis spectra characterizations

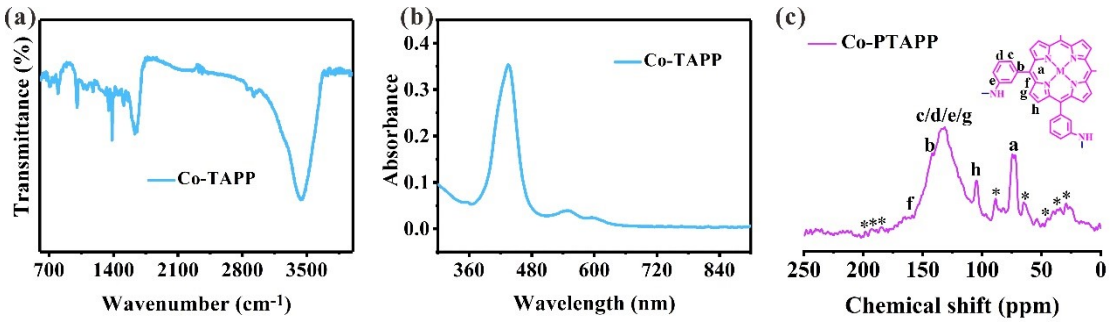

Figure S3. FT-IR spectra (a), UV/Vis absorptions of Co-TAPP (b), and Solid-state ^{13}C NMR of PTAPP (c).

As confined in Figure S3a, the vibration peak of Co-phenazine linkage in the FT-IR spectrum is not observed for Co-TAPP, further demonstrating that the Co-PTAPP occur the polymerization reaction. Compare TAPP and PTAPP, the number of Q-bands decreases to the two peaks, suggesting the coordination of Co atoms with the porphyrin ring and aminophenyl (Figure S3b). In Figure S3c, the Solid-state ^{13}C NMR revealed the phenazine linkages peak of Co-PTAPP at 131.5. (The asterisks indicate the side-peaks.)

Section S4 Electrochemical characterizations

4.1 ORR and OER curves of M-PTAPP

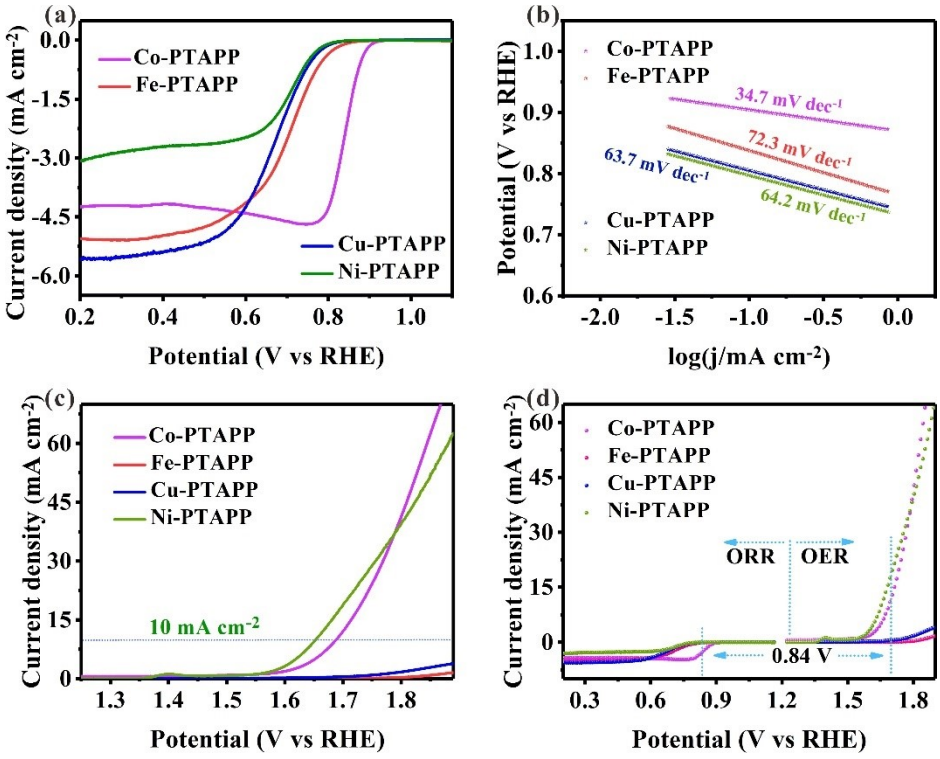

Figure S4. (a) LSV curves of M-PTAPP materials and (b) corresponding Tafel slopes. (c) OER polarization curves of M-PTAPP samples. (d) Combined ORR and OER for M-PTAPP catalysts.

In Figure S4a, the Co-PTAPP exhibits an outstanding $E_{1/2}$ and E_{onset}. Moreover, the calculated Tafel slope of Co-PTAPP (34.7 mV dec^{-1}) is markedly lower than Fe-PTAPP (72.3 mV dec^{-1}), Cu-PTAPP (63.7 mV dec^{-1}), and Ni-PTAPP (64.2 mV dec^{-1}), indicating the remarkable ORR activity and rapid kinetics of Co-PTAPP (Figure S4b). As shown in Figure S4c, the Ni-phenazine linkage active units significantly improves the OER performance. The Co-PTAPP molecular catalyst displays the superior bifunctional performance (Figure S4d).

4.2 CV tests in in N_2- or O_2-saturated alkaline electrolytes

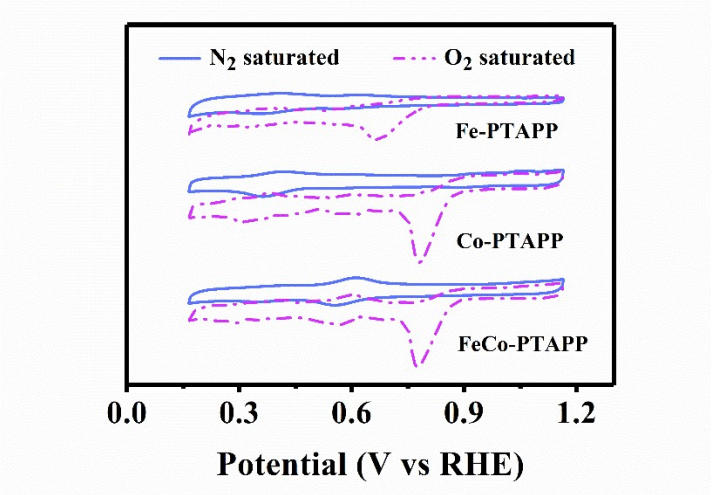

Figure S5. CV curves of Fe-PTAPP, Co-PTAPP, and FeCo-PTAPP.

Obviously, the Co-PTAPP material displays a high ORR performance. It clearly demonstrates that incorporating bimetal atoms into PTAPP have not further improve electrocatalytic activity (Figure S6).

4.3 The number of electron transfers

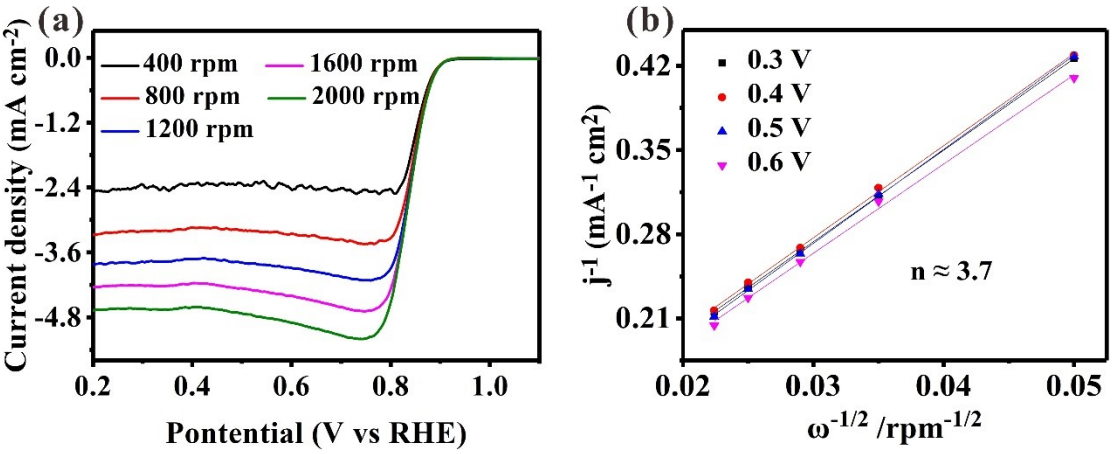

Figure S6. (a) Polarization curves at regular rotation rates (400 - 2000 rpm) for Co-PTAPP. (b) The K-L plots of Co-PTAPP material.

According to the KL equation in Figure S6a, b, the electron transfer number (n) of Co-PTAPP is calculated to be 3.7 in the region of 0.3-0.6 V.

4.4 ORR performance of Co-PTAPP and FeCo-PTAPP

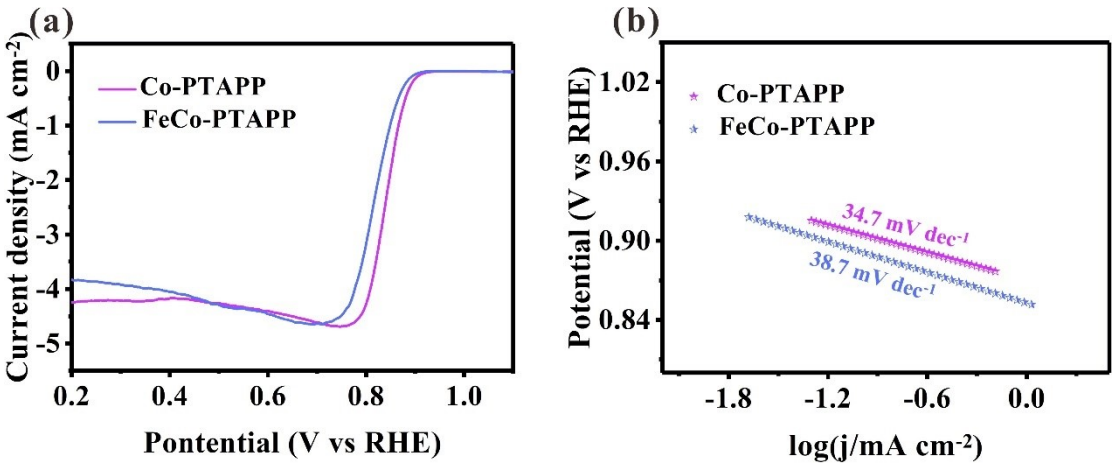

Figure S7. (a) LSV polarization curves. (b) Tafel plots.

In Figure S7, the Co-PTAPP catalyst presents a higher $E_{1/2}$ and E_{onset} than FeCo-PTAPP material. Moreover, the calculated Tafel slope of Co-PTAPP (34.7 mV dec^{-1}) is markedly lower than FeCo-PTAPP (38.7 mV dec^{-1}).

4.5 Methanol tolerance

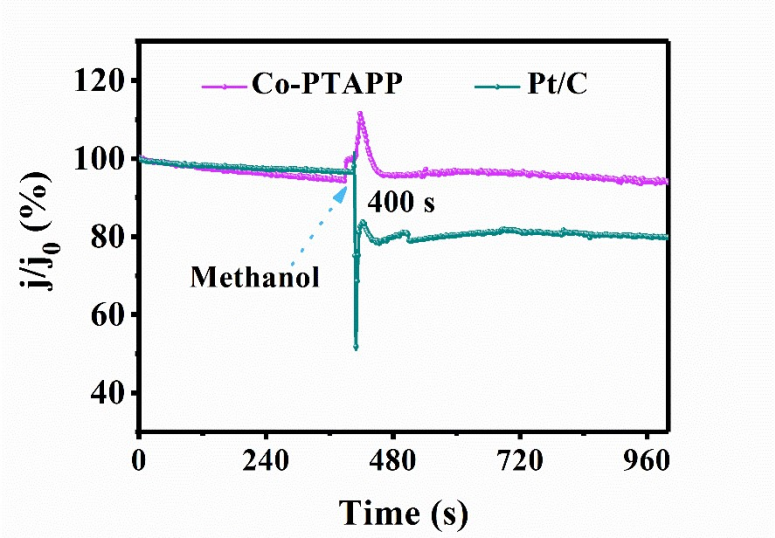

Figure S8. Methanol tolerance tests for ORR.

When 3M methanol is transfused into the 0.1 M KOH alkaline solution, the Pt/C catalyst exhibited a sharp shape change in the chronoamperometric measurements, indicating the occurrence of methanol oxidation (Figure S8). In remarkable contrast to Pt/C, the Co-PTAPP shows a stable chronoamperometry curve, implying outstanding methanol tolerance and potential in practical application.

4.6 The effective surface of Fe-PTAPP and Co-PTAPP

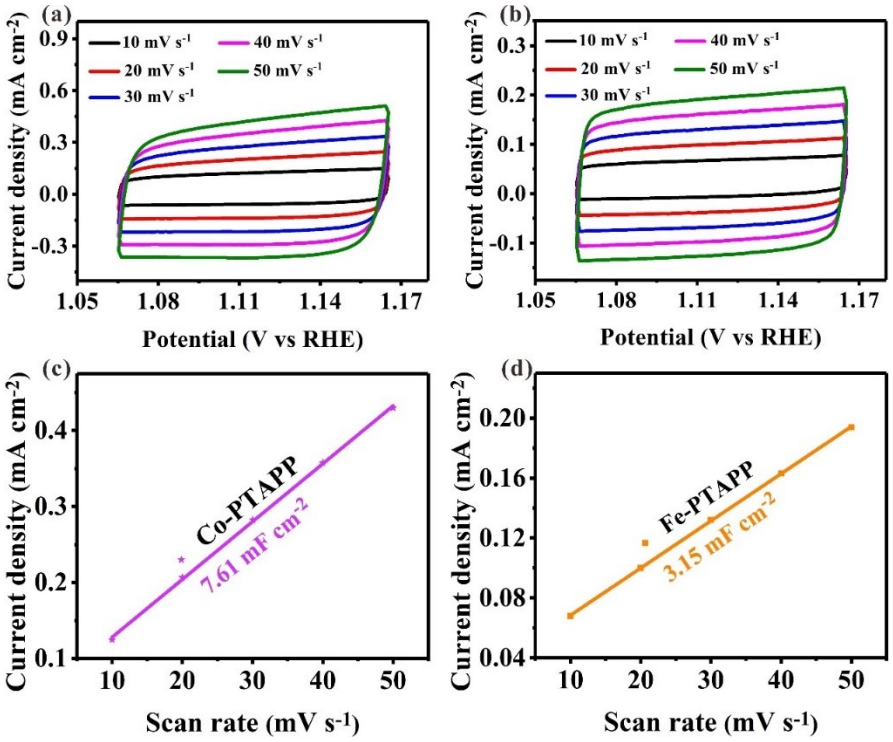

Figure S9. (a, b) CV curves of Co-PTAPP and Fe-PTAPP at different scan rate. (c, d) C_{dl} curve of Co-PTAPP and Fe-PTAPP.

In Figure S8, the C_{dl} value of Co-PTAPP is 7.61 mF cm^{-2} better than of Fe-PTAPP, indicating the more effective surface for Co-PTAPP.

4.7 The bifunctional activities

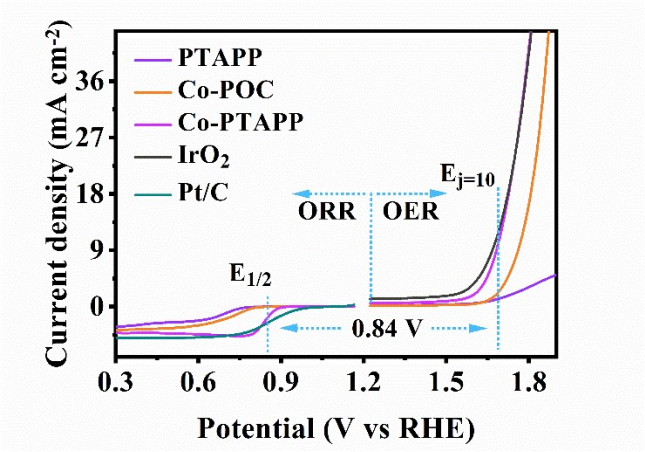

Figure S10 Combined ORR and OER for molecular catalysts.

Clearly, the Co-PTAPP molecular catalyst shows a lower value (ΔE = 0.84 V) than other sample catalysts (Figure S10d).

4.8 Tafel slopes

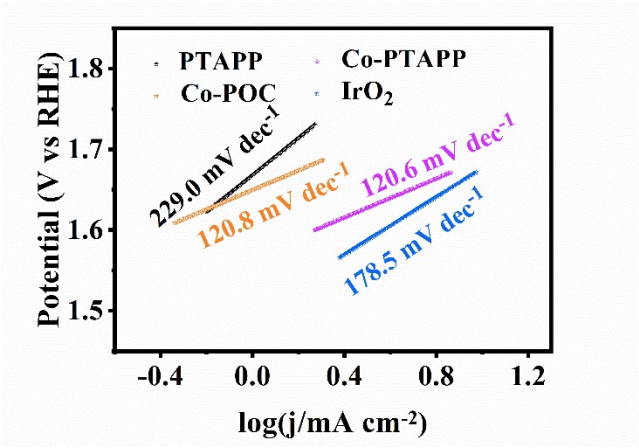

Figure S11. Tafel slopes of molecular and IrO_2 catalysts.

The Tafel slope of 120.6 mV dec^{-1} for Co-PTAPP is less than those of Co-POC (120.8 mV dec^{-1}), PTAPP (229.0 mV dec^{-1}), and IrO_2 (178.5 mV dec^{-1}), validating its better OER kinetics (Figure 5b).

4.9 The stability test of Co-PTAPP molecular catalyst

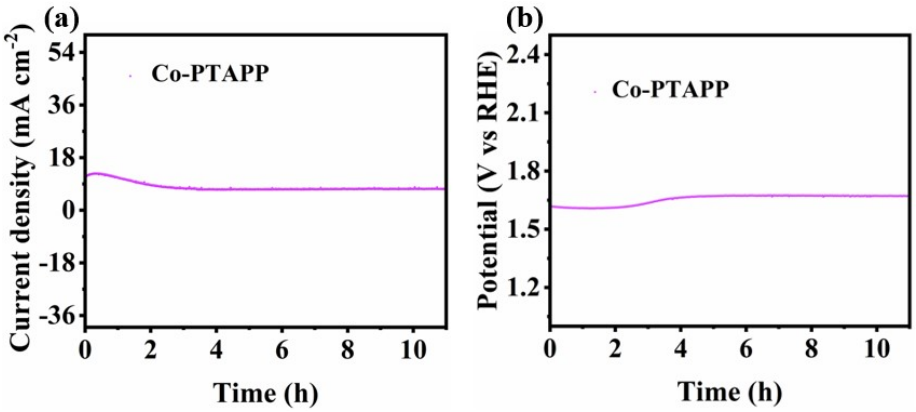

Figure S12 (a) Chronoamperometry tests for OER of Co-PTAPP at a potential of 1.624 V in 1.0 M KOH. (b) Long term stability test of OER for Co-PTAPP at 10 mA cm^{-2}.

4.10 The SEM images of Co-PTAPP material before and after testing

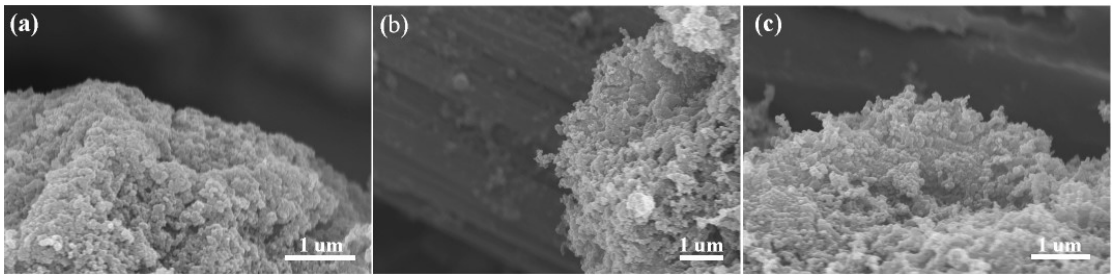

Figure S13 (a) SEM images of Co-PTAPP (a) before testing. (b) after I-t testing at 1.624 V. (c) after long term stability testing at 10 mA cm^{-2}.

4.11 The mapping images of Co-PTAPP catalyst after the OER test

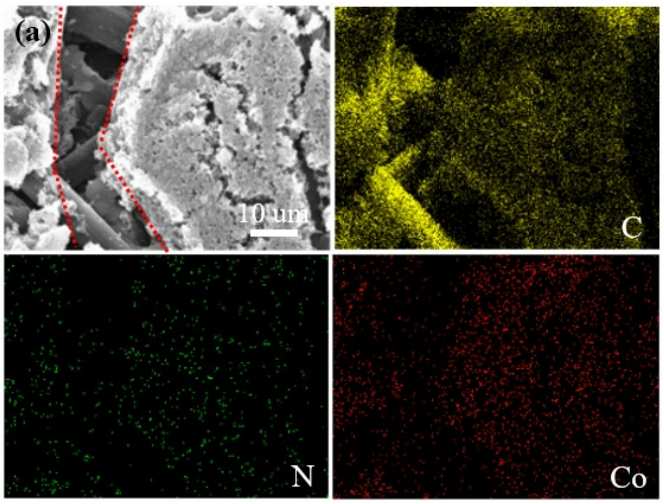

Figure S14 SEM image and mapping images of Co-PTAPP after the OER test.

4.12 The cell performance of the PTAPP, Ni-PTAPP, and Co-PTAPP

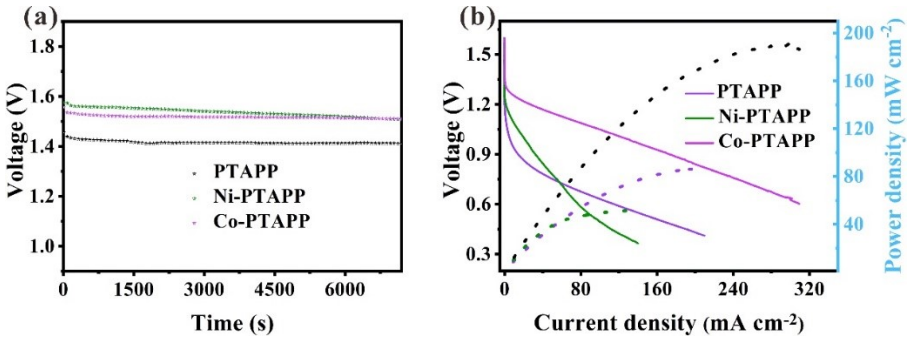

Figure S15. (a) OCV curves. (b) Discharge polarization curves.

The OCV for the Co-PTAPP-based ZAB is ≈ 1.53 V, which is higher than the PTAPP-based ZAB (1.36 V), confirming the significance of Co-N_2 bonding structure. Moreover, the Co-PTAPP-based ZAB exhibits an outstanding stability after 7200s than Ni-PTAPP catalysts (Figure S9). As described in Figure S9b, the Co-PTAPP-based battery exhibits a higher peak power density than other sample materials.

4.13 Water absorption process of HOEtMImCl

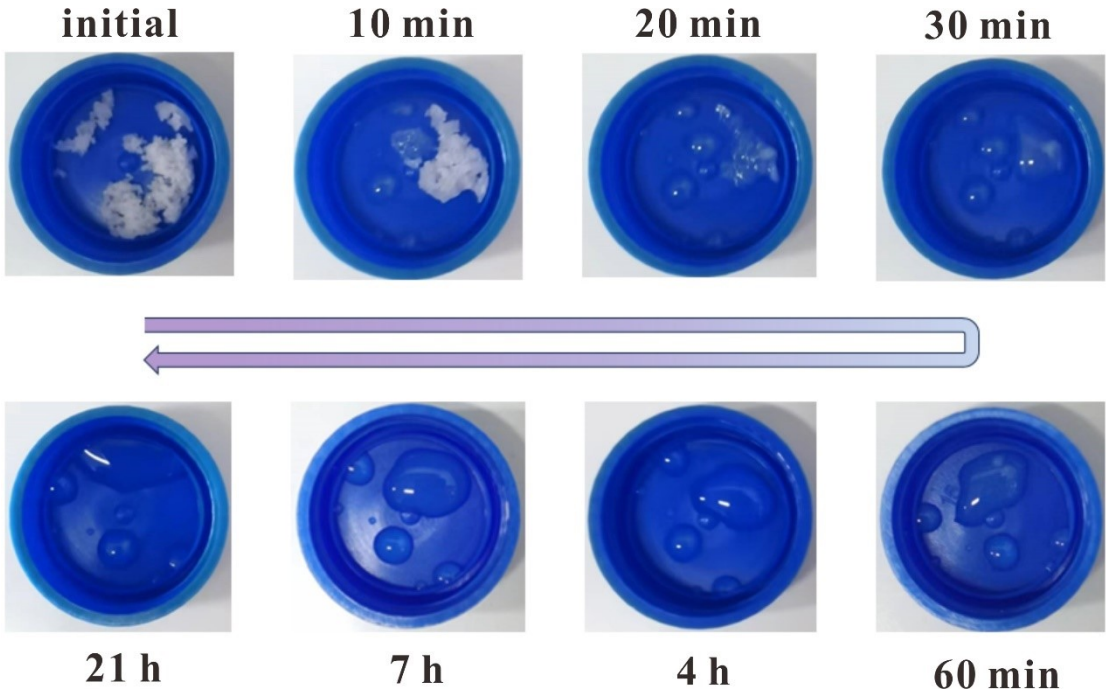

Figure S16. Optical images of HOEtMImCl in air atmosphere.

4.14 Water uptake value of HOEtMImCl

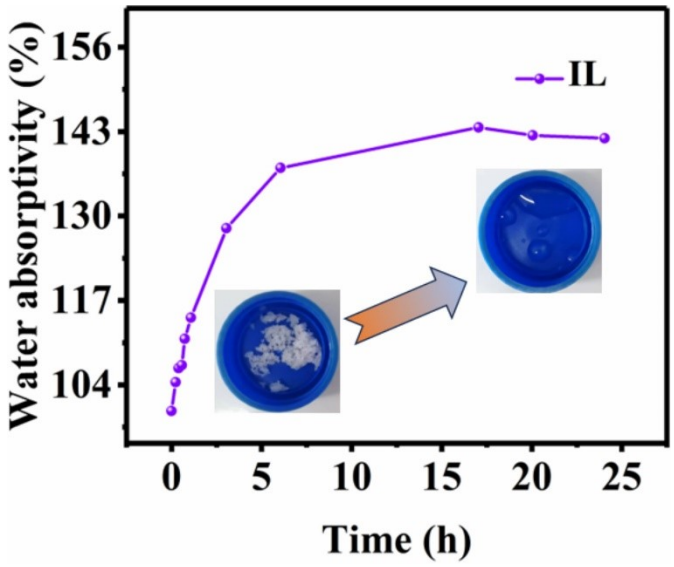

Figure S17. The measurement of water absorption for HOEtMImCl.

Table S1. Comparison of electrocatalytic performances between Zn-NC/GD sample and recently reported electrocatalysts applied in Zn-air batteries

Catalyst	Electrolyte (KOH)	$E_{1/2}$	Electrolyte (KOH)	$E_{j=10}$
Co-TPFPP/CNT[5]	0.1 M	0.760	1.0 M	1.710
Co-TPP/CNT[5]	0.1 M	0.810	1.0 M	1.680
CoP-TOB [6]	0.1 M	0.818	0.1 M	1.680
PNC-226 (Co)[7]	0.1 M	0.750	1.0 M	1.675
G@POF-Co[8]	0.1 M	0.810	0.1 M	1.660
CoTAPP-PATA-COF[9]	0.1 M	0.800	0.1 M	1.660
Co-TMPyP/CCG[10]	0.1 M	0.824	1.0 M	1.575
Co-POC[This work]	0.1 M	0.730	1.0 M	1.700
Co-PTAPP[This work]	0.1 M	**0.850**	**1.0 M**	**1.688**

References

[1] Kresse, J. Furthmuller, *Phys. Rev. B* **1996**, 54, 11169.

[2] J. P. Perdew, K. Burke, M. Ernzerhof, *Phys. Rev. Lett.* **1996**, 77, 3865.

[3] B. Hammer, L. B. Hansen, J. K. Norskov, *Phys. Rev. B* **1999**, 59, 7413.

[4] S. Grimme, *J. Comput. Chem.* **2006**, 27, 1787.

[5] H. Qin, Y. Wang, B. Wang, X. Duan, H. Lei, X. Zhang, H. Zheng, W. Zhang, R. Cao, *J. Energy Chem.* **2021**, 53, 77.

[6] J. Tang, Z. Liang, H. Qin, X. Liu, B. Zhai, Z. Su, Q. Liu, H. Lei, K. Liu, C. Zhao, R. Cao, Y. Fang, *Angew. Chem. Int. Ed. Engl.* **2023**, 62, 202214449.

[7] M. O. Cichocka, Z. Liang, D. Feng, S. Back, S. Siahrostami, X. Wang, L. Samperisi, Y. Sun, H. Xu, N. Hedin, H. Zheng, X. Zou, H.-C. Zhou, Z. Huang, *J. Am. Chem. Soc.* **2020**, 142, 15386.

[8] B. Q. Li, S. Y. Zhang, X. Chen, C. Y. Chen, Z. J. Xia, Q. Zhang, *Adv. Funct. Mater.* **2019**, 29, 1901301.

[9] M. Liu, S. Liu, C.-X. Cui, Q. Miao, Y. He, X. Li, Q. Xu, G. Zeng, *Angew. Chem. Int. Ed.* **2022**, 61, 2213522.

[10] K. Cui, Q. Wang, Z. Bian, G. Wang, Y. Xu, *Adv. Energy Mater.* **2021**, 11, 2102062.